Influence of the printing direction on the surface appearance in multi-material fused filament fabrication

Riccardo Tonello[1], Md. Tusher Mollah[1], Kenneth Weiss[1], Jon Spangenberg[1], Are Strandlie[2], David Bue Pedersen[1], and Jeppe Revall Frisvad[1,*]

[1] Technical University of Denmark, Kongens Lyngby, DK-2800, Denmark
[2] Norwegian University of Science and Technology, Gjøvik, NO-2802, Norway
*Corresponding author: jerf@dtu.dk

Abstract. Multi-material fused filament fabrication (FFF) offers the ability to print 3D objects with very diverse surface appearances. However, control of the surface appearance is largely a matter of trial and error unless the employed materials are very similar and very translucent, so we can think of them as blending together. When the multiple materials are fused into one filament in a diamond hotend extruder but do not blend, the resulting surface appearance depends on the printing direction. We explore how this leads to milli-scale colorations as a function of the printing direction. By having preferable printing directions, it is possible to exploit the limited color blending of this nozzle with multiple inlets and one outlet and further enhance particular color effects, such as goniochromatism. We present a framework based on both experimental and computational fluid dynamics analysis for controlling the extrusion process and the coloration of the surface according to preferable printing directions and mixing ratios with the aim of enabling fused filament fabrication of intricate surface appearances.

1 Introduction

Fused filament fabrication (FFF) is a popular technique for additive manufacturing because of its low cost. Color control has recently been explored in FFF by means of a diamond hotend extruder [27]. This extruder takes multiple filaments as input and outputs one fused filament (multiple-in-one-out nozzle). The principle is that the input filaments are conveyed into a mixing chamber where they merge. They then move to a transition zone where the temperature facilitates fusing of the filaments, and the nozzle deposits the fused filament onto the build plate. Song et al. [27] present an approach to produce reliable color gradients by fusing very translucent filaments so that the colors of the three filaments would seem to blend. In many cases, however, the colors of the fused filaments do not blend but rather mix.

When filaments combine to generate one mass with discernibly separated colors, we call it *mixing* as opposed to the indiscernible *blending* of filament colors

This version of the contribution has been accepted for publication after peer review but is not the Version of Record and does not reflect post-acceptance improvements, or any corrections. The Version of Record is available online at: https://doi.org/10.1007/978-981-99-9666-7_7

into a new color. This is a color analogy to the chemical use of the terms, where chemical mixing of constituents is reversible whereas blending is not. In this work, we study the visual effects of filament mixing instead of filament blending. Mixing of multiple colors or even multiple materials in one filament leads to intricate surface appearances, where the printing direction plays an important role with respect to the deposition of colors on the surface of a printed object.

Filament mixing occurs in a diamond hotend extruder when we have the right ranges of temperatures and pressures. The filaments then do not blend, and we can achieve color transitions along contours or shapes. Thus, as opposed to Song et al. [27], we start from the hypothesis that filaments in the nozzle tip do not blend with each other. We investigate the color deposition along each direction and exploit our findings to control color gradients by modulating the extrusion rate in each printing direction. In this way, by controlling mixing ratios and their variation, we carry out transition effects to create milli-size details not only in profiles and shapes but also in flat surfaces according to the printing direction. In a sense, our work enables a multi-color variant of the appearance fabrication technique by Chermain et al. [6].

2 Related work

Early work on color hatching and print direction was based on the use of multiple printing nozzles with a control on the azimuth angle for the printed part and the design of a tool-path planner [11]. Another approach involved dual-color (two-tone) texture-mapped surfaces [21], which were achieved by offsetting and overlaying different filaments in different layers. Following up on these ideas, Kuipers et al. [14] studied the linear halftoning principle of the prints to better control the transition of colors in objects. They used a dual extruder with switching of the tool-head to change colors. Also, Babaei et al. [4] used a multiple extruder machine. They found another way to optimize the process by computing the ink concentrations through an algorithm that provides a strict order of inks to the layers.

Alternatives to the multiple extruder system are the filament splicer [30], where different spliced filaments follow a designed tool-path planner to print multi-color, and ink FFF, where the filament is dyed according to its usage [12]. Filament splicing and inking are good for printing surfaces with patches of properly separated colors but do not enable effectively the combination of multiple colors or materials in one filament cross-section and the use of different tones from the filaments owned. Littler et al. [15] however achieved a mix of colors on a filament by applying ink from permanent markers. As a result, they observed differences according to the printing direction, but they also observed contamination of ink from marker to marker, and they did not describe a model for estimating the expected surface color as a function of the printing direction.

The diamond hotend technology we use has the advantage of fusing multiple filaments into one where the input filaments form a shared cross-section, but studies are mainly focused on how to reduce material usage and printing time [35]

Fig. 1. Retention of colors in 3D printed filaments.

or improve the segmentation between colors [36]. The work most closely related to ours is the work of Song et al. [27], but they mainly focus on the use of highly translucent filaments enabling color addition through strata.

3 Method

Fused filament extrusion is not a trivial problem. Many studies exist on the single extrusion process and the related fluid/melt dynamics [5,29,20,31,32,3,24,22,23], but we have been unable to find references on the multiple-in-one-out nozzle extrusion process. Hence, we developed a computational fluid dynamics (CFD) system to describe it.

3.1 Simulating the Multiple Extrusion Process

The process consists of multiple filaments conveyed into one tool-head with a hot end. Our setup is a multiple Bowden extrusion system, with three drive gears and one hot end. When two or more filaments are mixing at the tip of a nozzle with appropriate temperature and pressure, we obtain an extrude with retention of colors of the initial filaments, as depicted in Fig. 1. According to such evidence, we decided to investigate the correspondence between the color hatching and the print direction and exploit our findings to control color gradients by modulating the extrusion rate in each printing direction.

To find a simple geometric model for describing the extrusion process, we first use the tool FLOW-3D (Version 12.0; 2019; Flow Science, Inc.) [10]. We develop a novel Computation Fluid Dynamics (CFD) model to simulate the extrusion-deposition flow of multiple materials in FFF. According to literature, FLOW-3D was previously successful in predicting extrusion flows [17,22,16,8,28]. Our model comprises a cylindrical nozzle representing the tip of the E3D V6-nozzle, and a static substrate/build plate, as seen in Fig. 2 (left). We consider a nozzle speed of 50 mm/sec and a layer thickness of 0.3 mm. In the case of multi-material representation, our model uses three mass sources occupying the nozzle orifice equally. The locations of these are at the top of the nozzle (Fig. 2, left). Material

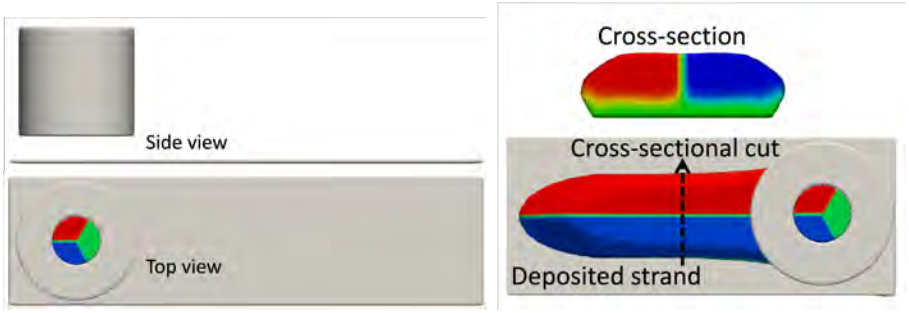

Fig. 2. Geometry of the CFD model (left). The hotend is visible from the side and top view with its extrusion tip and three mass sources in it and the substrate. Post-processing of a simulated result (right).

i for $i = 1, 2, 3$ has a source of fluid with its own scalar concentration value ψ_i corresponding to its color.

The extrusion-deposition flow of the multi-material was modelled as a transient and isothermal Newtonian fluid, as modelled in [7,26,25,18]. Those are sufficient assumptions to predict the strand size observed in the experiments. The continuity, momentum, and scalar transport equations governing the flow dynamics then become

$$\nabla \cdot \mathbf{u} = 0\,, \tag{1}$$

$$\rho\left(\frac{\partial \mathbf{u}}{\partial t} + \mathbf{u}\cdot\nabla\mathbf{u}\right) = -\nabla p + \eta\nabla^2\mathbf{u} + \rho\mathbf{g}\,, \tag{2}$$

$$\frac{\partial \psi_i}{\partial t} + \mathbf{u}\cdot\nabla\psi_i = D_i\nabla^2\psi_i\,, \tag{3}$$

where $\mathbf{u}$ is velocity, p is pressure, t is time, ρ is density, $\mathbf{g}$ is the body acceleration vector, and η is the constant viscosity of the Newtonian fluid. We use $\rho = 1240$ kg·m^{-3} and $\eta = 1000$ Pa·s. In the transport equation, ψ_i denotes the scalar concentration (mass per fluid volume) of input filament i and D_i is the diffusion coefficient. The latter is approximated by

$$\rho D_i = \frac{\eta}{S_c} + \psi_{c,i}\,, \tag{4}$$

where S_c is the Schmidt number and $\psi_{c,i}$ is a constant scalar concentration for input filament i. This model describes how the colored materials move.

We use the finite volume method (FVM) and discretize the computational domain of the model using a uniform Cartesian grid. The bottom plane of the model contains a non-moving solid substrate, meaning that the plane has a wall boundary condition. The nozzle orifice at the top plane has an inlet boundary that includes the mass sources. We give other planes a continuative boundary condition. The fluid can then escape the computational domain, but the domain is large enough to keep the fluid inside it. Solid objects that can touch the

fluid have a no-slip boundary condition. The pressure and velocity components are solved implicitly in time. The momentum and scalar advection are calculated explicitly with second-order accuracy in space and first-order accuracy in time. Furthermore, we model the free surface using the volume of fluid (VOF) method [34,9]. Moreover, we set the time step size to be dynamically controlled based on stability criteria during the simulations in order to avoid numerical instabilities [10], where we set an initial minimum value to 10^{-5}.

To visualize a 3D strand simulated using our method and to present 2D cross-sections of deposited strands, we use the post-processing tool FLOW-3D POST [10]. A result is in Fig. 2 (right). The material coming from a mass source has an integer scalar concentration value representing its color (red = 3, green = 2, blue = 1). When the fluid fraction is visualized the three colors are blended showing a smooth transition from one color to another. These color transitions in the simulated results are a consequence of both numerical and scalar diffusion that also take into account the scalar fraction in a given control volume.

3.2 Geometric Color Distribution Model

Based on our simulations, we came up with a simpler geometric model to describe the distribution of colors for different print directions. The idea is based on the filament material cross section at the nozzle tip over the build plate, where the three filaments occupy space according to their grade of homogeneity and their chosen mixing ratios. The motion of the nozzle tip across the build plate and along a chosen direction was thought of as a repetition of the same projection pattern with its overlay, causing the mix of the filaments.

In the model, the extrusion tip is ideally divided into 12 circular sectors with a top angle of 30° and construction lines that are traced for each angle formed in this way. The construction lines are traced following a geometrical approach and they hence approximate the actual conformation of the colored filament melts in the nozzle tip. The straight continuous lines passing through the centre O are the main construction lines and their intersection with the circumference generates two points for each angle. The parallel dashed lines to the main construction lines represent the secondary construction lines and complete the design, as depicted in Fig. 3 (left). For each angle, there is one main construction line and four secondary lines, dividing the tip into six parallel sections. The model was designed with an ideal mixing ratio of 33.3% for each filament. We took advantage of these six sections in order to compute the occupation of the space between the three filaments. The division into sections also helps quantify to what extent the filaments do not mix. Assuming cyan, magenta, and yellow input filaments, we calculate expected CMYK colors using ratios of the areas of each filament relative to the whole area section.

As an example, we show the section $\overline{ABEF}$ along the direction at 0° with the vertical axis (Fig. 3, left). In this section, the two colors are not occupying the same percentage of space and the difference is given by the triangle $\triangle HOK$, where H is found at the intersection between the construction line traced from B to E and the segment $\overline{OC}$ originating from the perpendicular bisector of the

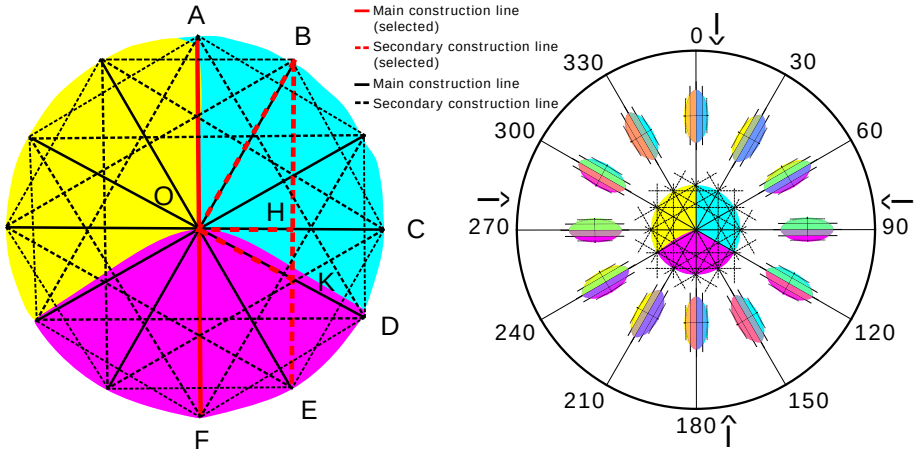

Fig. 3. Geometric division of the nozzle tip (left) approximating the distribution of the colored filaments. Analytic assessment of the color distribution upon extrusion (right) according to the printing direction (arrows).

construction lines along the chosen direction, and K at the intersection between $\overline{BE}$ and the segment of a construction line that matches the boundary between the two colors. Considering the area of the section $\overline{AOHB}$ as a unit, the area of the section $\overline{AOKB}$ defines a directional coefficient x:

$$x = \frac{A_{AOB} + A_{BOH} + A_{HOK}}{A_{AOB} + A_{BOH}} = \frac{\frac{r^2\pi}{12} + \frac{\sqrt{3}r^2}{8} + \frac{\sqrt{3}r^2}{24}}{\frac{r^2\pi}{12} + \frac{\sqrt{3}r^2}{8}}\,, \tag{5}$$

where the radius of the nozzle tip r cancels out, and we have $x = 1.15$ giving 15% more cyan than magenta in the $\overline{ABEF}$ section. Generalizing this method, we can find the areal fraction of a color in one half of a section of interest. We choose half sections to enable the use of different weights for front and rear parts of the cross section, as we can see in the example simulation in Fig. 2 (right) that the material in the rear part of the nozzle tip with respect to the printing direction comes out on top. Selecting a uv-coordinate system, where v is the (negated) printing direction and u is perpendicular to this, the result for a section from u_1 to u_2 is

$$x = \int_{u_1}^{u_2}\int_{f(u)}^{\sqrt{r^2-u^2}} \mathrm{d}v\,\mathrm{d}u \;\Big/\; \int_{u_1}^{u_2}\int_{0}^{\sqrt{r^2-u^2}} \mathrm{d}v\,\mathrm{d}u\,, \tag{6}$$

where $f(u)$ is the color separation, that is, a curve that cuts the section of interest. In the case of a straight line cut (as in Fig. 3), we can use the material division angle θ_c between two colors to find the slope of the line. Measuring the division angle θ_c from the v-axis, we have

$$f(u) = \frac{\cos\theta_c}{\sin\theta_c}u\,. \tag{7}$$

We found parametrization of a section by angles with the v-axis more convenient. This means that $u = r \sin\theta$, and we use $\sin\theta_1 = u_1$ and $\sin\theta_2 = u_2$. Another way to write (6) is then

$$x = \frac{\int_{\theta_1}^{\theta_2} \left(\cos^2\theta - f(\sin\theta)\cos\theta\right) \mathrm{d}\theta}{\int_{\theta_1}^{\theta_2} \cos^2\theta \,\mathrm{d}\theta} \tag{8}$$

$$= 1 - 2\frac{\int_{\theta_1}^{\theta_2} f(\sin\theta)\cos\theta \,\mathrm{d}\theta}{\theta_2 - \theta_1 + \frac{1}{2}(\sin(2\theta_2) - \sin(2\theta_1))}\,. \tag{9}$$

Using the straight line cut in (7), the formula becomes

$$x(\theta_1, \theta_2, \theta_c) = 1 - \frac{\cos\theta_c}{\sin\theta_c} \frac{\cos^2\theta_1 - \cos^2\theta_2}{\theta_2 - \theta_1 + \frac{1}{2}(\sin(2\theta_2) - \sin(2\theta_1))}\,. \tag{10}$$

The full section example in (5) is obtained with parameters $\theta_1 = 0, \theta_2 = \frac{\pi}{6}, \theta_c = \frac{2\pi}{3}$. For half sections, the division angle θ_c will be smaller than $\frac{\pi}{2}$ and x becomes the fraction of the half section occupied by a color.

Colors along different directions are dithered in a way that makes the load factor difficult to establish. One should consider color loss due to the layer thickness, the optical properties of the materials, and the coating coefficient of the lower material (excluding the effect of the substrate) [13]. In this study, these aspects are not precisely described. We approximate our color filaments with a percentage range from 0 to 100, where 0 is the absence of a color and 100 means fully used. Thus, using the CMYK (c, m, y, k) model, we have the boundary condition:

$$c + m + y \leq 100\,. \tag{11}$$

We exclude black (k) as it is currently not available in our printer, and we consider each of c, m, y a linear interpolation of two evaluations of (10) (x converted to percentage) with blending parameter a. The two evaluations are for the two half sections with parameters corresponding to the section of interest (θ_1, θ_2) and the material division angle (θ_c) in this section.

Based on our perception of translucency of the input filaments we use and on the distribution of material in the output filament of our simulations (Fig. 2, right), we selected a blending parameter of $a = \frac{10}{17}$. This factor is used for the rear half section of the material in the nozzle cross section because the simulation demonstrates that this comes out on top. For the example in Fig. 2 (right) with the nozzle moving downwards, the linear interpolation of the areas with colors in the two half sections is

$$\begin{aligned} c &= (1-a)\, c_{\text{front}} + a\, c_{\text{rear}} \approx \tfrac{7}{17}\, 0.15 + \tfrac{10}{17}\, 1 = 0.65 \\ m &= (1-a)\, m_{\text{front}} + a\, m_{\text{rear}} \approx \tfrac{7}{17}\, 0.85 + \tfrac{10}{17}\, 0 = 0.35\,, \end{aligned}$$

where $m_{\text{front}} = x(0, \frac{\pi}{6}, \frac{\pi}{3})$ and $c_{\text{front}} = 1 - x(0, \frac{\pi}{6}, \frac{\pi}{3})$. The resulting CMY color is then (65, 35, 0). Fig. 3 (right) illustrates the result of evaluating our geometric model for 12 different printing directions. Table 1 lists the colors of all the

Table 1. CMY values for each section per printing direction.

P.direction/Section	1	2	3	4	5	6
0°	(0,0,100)	(0,18,82)	(0,35,65)	(65,35,0)	(82,18,0)	(100,0,0)
30°	(0,0,100)	(0,0,100)	(32,23,45)	(59,41,0)	(59,41,0)	(59,41,0)
60°	(0,0,100)	(26,0,74)	(50,0,50)	(50,50,0)	(26,74,0)	(0,100,0)
90°	(59,0,41)	(59,0,41)	(59,0,41)	(32,45,23)	(0,100,0)	(0,100,0)
120°	(100,0,0)	(82,0,18)	(65,0,35)	(0,65,35)	(0,82,18)	(0,100,0)
150°	(100,0,0)	(100,0,0)	(45,32,23)	(0,59,41)	(0,59,41)	(0,59,41)
180°	(100,0,0)	(74,26,0)	(50,50,0)	(0,50,50)	(0,26,74)	(0,0,100)
210°	(41,59,0)	(41,59,0)	(41,59,0)	(23,32,45)	(0,0,100)	(0,0,100)
240°	(0,100,0)	(18,82,0)	(35,65,0)	(35,0,65)	(18,0,82)	(0,0,100)
270°	(0,100,0)	(0,100,0)	(23,45,32)	(41,0,59)	(41,0,59)	(41,0,59)
300°	(0,100,0)	(0,74,26)	(0,50,50)	(50,0,50)	(74,0,26)	(100,0,0)
330°	(0,41,59)	(0,41,59)	(0,41,59)	(45,23,32)	(100,0,0)	(100,0,0)

sections for each printing direction, and section counting is from left to right taken with respect to the printing direction.

For a particular extrusion direction, the profile of pressure is different for the front and the rear part of the tip [1,24,7]. In fact, the synergy of the fan, placed above the nozzle to control and keep the temperature as uniform as possible, and the printing direction strengthen the uplift of the melt outside the projection of the tip and provide an additional gradient of force to the momentum. For a selected printing direction, the melt has a higher uplift in the front part because of the friction force. This generates a profile where the pressure of the melt at the tip is lower than the one at the contact point with the build plate. In this way, the rear part, which has thus a lower uplift of the melt outside the projection of the tip, receives a slight upward pressure that covers the front part. However, this is not always consistent because the pressures in the nozzle are, on average, higher than the ones in normal one-nozzle FFF and the optimal range of those is narrower. It is thus more frequent in our case to have melt fracture or sharkskin instabilities [24].

The extrusion process is also related to the filament feed. In particular, according to the volume continuity equation (1), the volume of the material entering the nozzle tip must be equal to the volume of material extruded from the outlet. Thus, we write the formula for the filament feed E_{step} as

$$E_{\text{step}} = \frac{4whL}{\pi d^2}\,, \tag{12}$$

where h is the height of the layer, w is the extrusion width, L is the length of the filament extruded (with relation to E), and d is the filament diameter [2].

4 Experiments and Visualization

We followed a trial-and-error method [1] to find the temperature, flow rate, and print speed that would meet our objective of having filaments in the nozzle tip

Fig. 4. Radial dodecagon. Photos of the central radial structure seen from above (middle left) and the entire part (middle right). Visualization of the radial dodecagon from above (far left) and the entire part (far right). We rotated the sample to have the colors in the different strands comparable to the colors in Fig. 3 (right).

that mix but do not blend. The outflow of the melted filaments is then only one filament with separated phases according to the chosen mixing ratios. To test our theories, we implemented a custom slicer with a tuning of the rotation of the gears in the stepper motor drivers by generating a computer numerical control script (G-code). We followed the approach of having all three extruder drivers enabled and making them work weighted according to the equation:

$$\sum_{j=1}^{n} w_j = 100\,, \tag{13}$$

where w_j is the weight of extruder j and n is the number of extruders. We set the sum to 100 to indicate 100% of the the nozzle tip volume. To apply these weights correctly to the diamond hotend technology, we consulted Spiritdude's Public Notebook [19]. We converted the mixing ratios to the G-code format through the use of A, B and C, used in CNC machines as rotational axes around X, Y and Z. We used a three inlets diamond hotend 3D printer and poly-lactic acid (PLA) filaments of different colors. The nozzle was an 0.4 mm single nozzle with a standard 40 watts cartridge heater. The board was RAMPS 1.4 EFB (i.e. the connections are for E-extruder, F-fan and B-build plate) with architecture Arduino ATmega2560 and stepper expander and we configured the board with Marlin 2.0.8. The build plate was not heated for the entire process because the material of the build plate was sticky enough to facilitate the deposition without incurring warpage or problems during the process. We set the printing temperature at 220 °C and the nozzle speed at 50 mm/sec while feeding the nozzle with 1 mm of material.

To test the accuracy of our geometrical model and the feasibility of using it as a base for a visualization tool, we printed a prism with a radial dodecagonal base. Every layer was printed with a radius starting from the centre and culminating in each vertex of the dodecagon and a broken line connecting all the vertices. The printed part is in Fig. 4. By constructing this radial dodecagon, it appears that some print directions have the coalescence of all three colors, while others are more stable and easier to predict. Moreover, opposite print directions have slightly different colors. Overall, the printed part correlates quite well with the

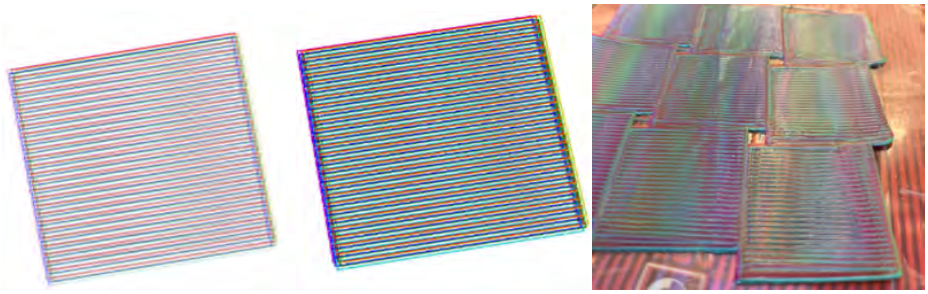

Fig. 5. Visualizations (left and middle) and prints (right) of a square with 10° inclination and (33,34,33) color combination. Visualizations show the difference between 2D (left) and 3D (middle) with color mixing and alpha channel adaptation. The printed parts exhibit milli-scale coloring effects.

simple geometrical model and we then designed a visualization system based on the sections depicted in the geometrical model (Fig. 3, right), in order to predict beforehand the outcome for other surfaces.

The strategy adopted is based on a custom 3D printer simulator with the assumption that the deposition of colors works according to the FLOW-3D model described before, related to the juxtaposition of the strands, and to our geometrical model for the placement of blended sections in between. In addition, we considered the non-extrusion movements of the tool-head an active part of the printing process, as the oozing effect may occur. The visualization of the digital twin is in Fig. 4.

We followed a similar approach for flat surfaces. Printing on flat surfaces and retaining the same optical effect require different specifics. In this regard, we took advantage of the construction lines and the difference in color between two opposite directions in Fig. 3 (right). Thus, we took into consideration the fact that during the quick non-extrusion movements in the printing process, the tool-head suffers from oozing while retracting the filament due to the gradient of pressure at the nozzle tip. Thus, in our visualization system, we considered the GO linear movement (G-code) as an extrusion movement as well, even though it has a limited impact on the final appearance. Moreover, we included the mixing of the filaments, although all the tests have been conducted on equidistant parallel lines. The borders and the proximity between lines can dirty the tip and drag undesired color onto other parts of the prints. Assuming so but neglecting it, we first visualized the effect by adding these properties to our tool: we created the coloring effect by considering as extrusion points the non-extrusion ones and we added mixing lines only at the interfacial portions between filaments.

Moreover, we added the effect of the colors due to the extrusion weights by including the alpha channel to have a more realistic effect on the prints. The final result is visible in Fig. 5. In order to plot in 3D the desired effect, we added a plotting scheme according to the minimum distance from the camera, as well as for the line thickness. We changed the layer thickness according to the camera distance. The maximum camera distance was set at 10 and the minimum at

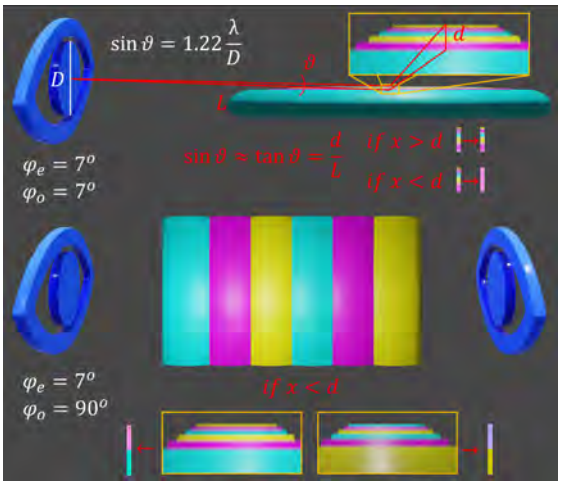

Fig. 6. Top: Angular resolution of an eye, where ϑ is the smallest resolvable visual angle ($1/\vartheta$ is the visual acuity), D is the diameter of the pupil, λ is the wavelength of the light, while L and d are the distance to and the height of the detail. Bottom: Schematic representation of the change of view in a multi-color 3D printed patch with a detail, x, below the threshold d (loss of acuity). The angles φ_o and φ_e are respectively your elevation as observer and the elevation of the eye in the figure.

4.5, as well as the maximum line thickness at 4 and the minimum at 1. This operational range was due to the choice to have the entire visualization of the part and not just a detail. In addition, when the line thickness is too big, the last plotted line superimposes all the others and this is not what we desired when, according to the geometrical and the physical model, we had different colors distributed in every hatch. Finally, as the last step of our pipeline, we printed what was found with the visualization tool. All the parameters used before for the radial dodecagon have been kept here as well. Results are displayed in Fig. 5.

5 Visual Effects

The design of a part can create very different color effects. When looking at a filament from a distance, we cannot clearly distinguish one point on the filament surface from another. The visual acuity of a human is limited. It is considered an areal patch subtending the smallest possible solid angle that we can distinguish [33]. When observed at some distance, this minimal discernible area covers several different colors that we will perceive as one color (at 1 m distance the patch has a width of 0.136 mm). If we look at the filament from a different angle, the ratio of different colors in the patch can change causing us to see a different color (Fig. 6). This leads to goniochromatism, which we sometimes observe in our mixed filaments.

The design of the print path is essential for reproducing this effect. When printing vertically with a circular pattern, the filaments are deposited one upon

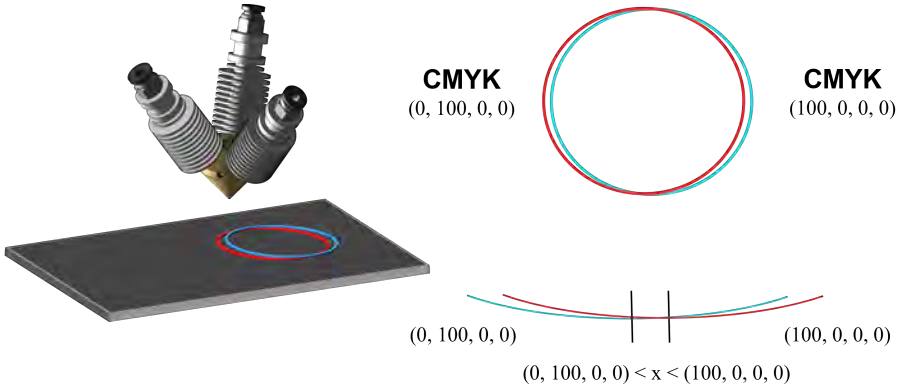

Fig. 7. Visualization of the process for rounded shapes.

another and this limits the visibility of the top part of the strands. Moreover, the filaments are not printed concentrically but they are slightly offset because of the uncompleted blending at the nozzle tip. In this way, in turn, from an external position along the trajectory, they gradually move inward to reach the internal position, and vice-versa. This particular pattern creates two blended zones where the filaments are moved transversely with respect to the portion of the nozzle tip they occupy (Fig. 7). In a flat surface instead, the goniochromatism is based on the juxtaposition of the filament strands so that it is possible to create such optical effects according to the change in the elevation of the observer.

6 Results and Discussion

We applied our CFD model to multi-material deposition in four different printing directions. In Fig. 8, we present the simulated strands and their cross sections taken midway along each strand. These results clearly demonstrate that the printing direction influences the distribution of colors in a strand and, as a consequence, it will influence the colors that appear on the surface of a printed object too. The position of each color in the filament is clear. If we let the green color in this simulation represent yellow in our geometric CMY model (Fig. 3, right), the positive X-direction in the simulation corresponds to 120 degrees in the geometric model, the negative Y-direction corresponds to 210 degrees, and so forth. The distribution of colors seen in the simulation thus matches our simplified geometric model fairly well.

3D-printing goniochromatic-like surfaces with a multi-material FFF printer requires the calibration of several parameters. The selection of the correct slicer is fundamental to control effectively the deposition of material. We designed and assessed three custom slicers to be able to control the flow rate during extrusion and have multiple filaments in the nozzle tip that do not blend. They were based on computer numerical control scripts (G-code), which input precise commands

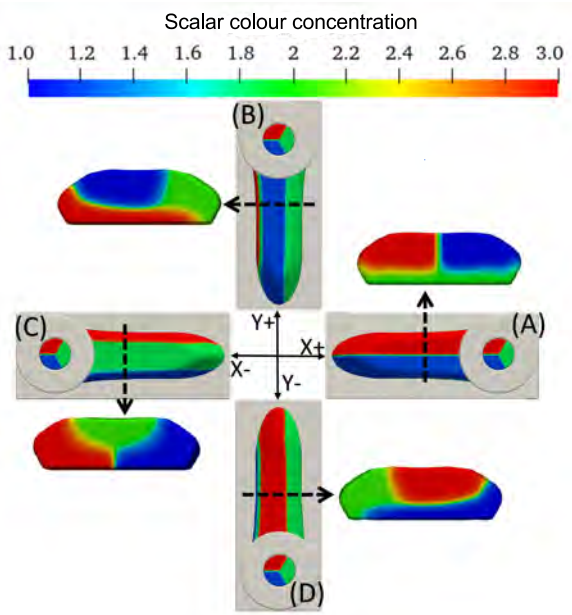

Fig. 8. Strands of multi-material printing and their cross sections for different printing directions: (A) positive X-direction; (B) positive Y-direction; (C) negative X-direction; and (D) negative Y-direction.

for the gears. An example of extrusion along the x-axis is as follows:

$$\mathbf{G}1\,\mathbf{F}500\,\mathbf{X}50\,\mathbf{Y}50\,\mathbf{Z}0\,\mathbf{E}10 \Rightarrow \mathbf{G}1\,\mathbf{F}500\,\mathbf{X}100\,\mathbf{Y}50\,\mathbf{Z}0\,\mathbf{E}20\,,$$

where **X**, **Y**, **Z** are the coordinates of the system taken into account, **G** is the command for the linear movement, **F** is the tool-head speed and **E** is the extrusion rate, E_{step} in (12). Moving the extruder from point to point, in order to have a continuous flow, we had to increase the length of the filament that enters the extruder. By changing the value of the E_{step} in the illustrative string above, it was possible to modulate the filament flow and the extrusion process itself. The G-code file enables both an easy switch between different extruder drivers or the simultaneous use of them. We thus tested three different approaches to find the better method for carrying out prints with milli-scale precision (Fig. 9).

In our first approach, the extruder switched after a fixed amount of points by turning them off and on when desired. This method (Fig. 9, left) was the easiest to implement, but it gave a delay due to the continuous change of pressure in play and it was not possible to extrude effectively by switching the motor driver at every string.

In our second approach, we divided the difference between two strings for the **X**, **Y**, **Z**, and E_{step} values into a pre-selected number of parts and an additional string was generated for each of these segments. This enabled the creation of sub-strings that could improve the resolution and reduce the delay between points.

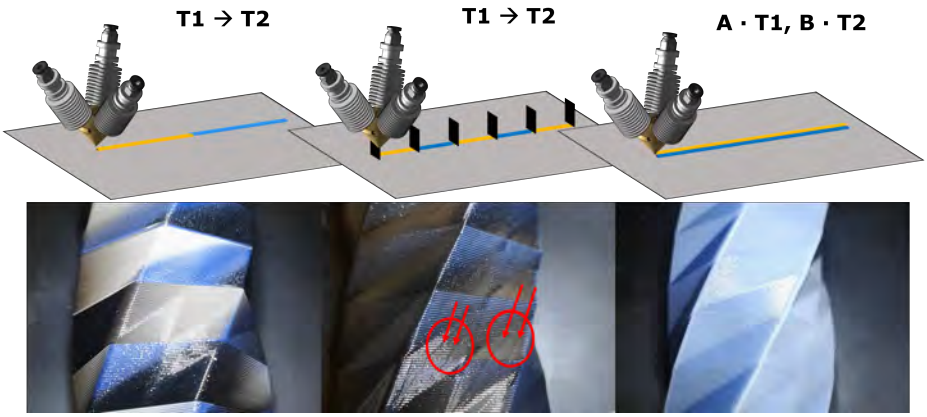

Fig. 9. The three implemented approaches. T1 → T2 represents the switch from the T1 extruder (in orange) to the T2 extruder (in blue). A and B represent the mixing ratios for each extruder in the third approach. In red inaccuracies such as wrinkles.

The switch was weighted according to (13) and the sub-string was found using

$$a_i \leq a_{i+k} \leq a_{i+1}\,, \tag{14}$$

where a_i is the point in the Cartesian coordinate system given by a single string in the G-code and $a_{i+1} - a_i$ is the segment generated in this way with two different strings, k partitions the segment in sub-segments. This method is not good for corners and edges because it adds additional artefacts in the texture, such as bulges and wrinkles, as shown in Fig. 9 (middle).

Our third approach (the one we used for all other results) consists of having all three extruder drivers enabled with the mixing ratios as we previously discussed. To assess the quality attainable with these three approaches, we printed a twisted vase with dimensions of $40 \times 40 \times 80$ mm with a hexagonal base and vertical edges connecting to the subsequent vertex of the projected base at the top (Fig. 9). The third approach attains the best quality for our purposes, but it is still influenced by additional parameters that we did not take into account, such as the use of a fan attached to the tool-head and its vibration profile.

While for vertical surfaces the primary design parameter that could affect the outcome is the layer thickness, since the responsible for the optical effects is the mechanism of the machine itself, for flat surfaces, there are many more. For instance, if the parameters such as printing speed, temperature and retract length are not set correctly, the surface presents irregularities and the strands are not visible, as well as any consistent optical effect, except for those ones related to the material (Fig. 10B).

Thus, in our visualization model, we also took into account different design parameters that are not directly related to the extrusion process but affect the final appearance of the part. In fact, we focused on air gaps, which are fundamental in the design of optical effects. Sparsely printed strands show only the

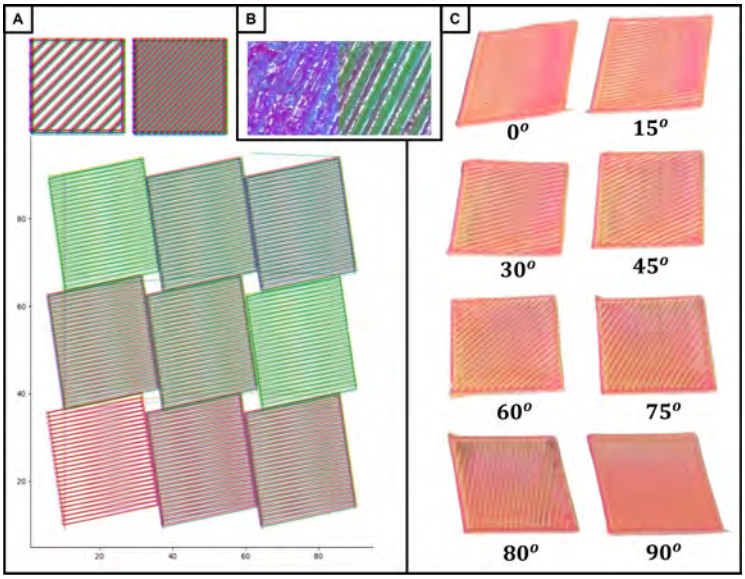

Fig. 10. A) Using our visualization tool for squares with different air gaps and raster angle of 45° (top left) and the series of squares in Fig. 5 with 10° inclination from the x-axis and different extrusion weights (bottom left). B) First tests for creating optical effects of flat surfaces. The left image has temperature, retract length, print speed and air gap not optimized, whereas the right image has optimized parameters. C) Printed squares with different printing directions.

retention of colors of the filaments and do not create any particular effect other than just a series of alternating colors. Also, mixing ratios or extrusion weights have a strong influence on the final tone of color, as depicted in Fig. 10A.

In Fig. 10A, the series of tests with the direction slanted of 10° from the horizontal ideal 0° line combines different color combinations, according to different extrusion weights. From the bottom left corner, each square acquired 10% of the third color for a maximum of 50%, starting from (0,50,50) where the suggested base follows the CMY model (i.e. (10,40,50), (20,30,50), ..., (50,0,50), (50,10,40), ..., (50,30,20)). However, one of the most important parameters that affect appearance is the printing direction, as depicted in Fig. 10C. These results demonstrate that a part can visually change by modifying details in the design setup. The layer thickness, the air gaps, the selection of the slicer, the mixing ratio as well as the optimal flow rate and more importantly the printing direction can have a big impact on the final appearance of the part (Fig. 10C).

7 Conclusion

We presented a CFD method for simulation of the multi-material flow in a diamond hotend nozzle. This is useful for predicting the influence of printing

direction on the distribution of materials in the output from such a multiple-in-one-out nozzle. Based on this simulation tool, we proposed a simple geometric model for describing the color distribution in a printed filament as a function of the printing direction. In addition, we developed a visualization tool based on line drawing to provide an indication of the color distribution on the surface of a printed object as a function of the designed computer controlled tool path (G-code). Using a printed radial dodecagon, we found a reasonable correlation with the prediction of our geometric model and our visualization tool. We found the printing direction useful with respect to performing milli-pigmentation control when using a multiple-in-one-out nozzle (diamond hotend) technology. Finally, we suggest a more precise quantification of the effects of both printing direction and change of the mixing ratio in future work.

Acknowledgements This work is part of the ApPEARS project funded by the European Union's Horizon 2020 programme under the Marie Skłodowska-Curie Actions grant agreement no. 814158.

References

1. Agassant, J.F., Pigeonneau, F., Sardo, L., Vincent, M.: Flow analysis of the polymer spreading during extrusion additive manufacturing. Additive Manufacturing **29**, 100794 (2019). https://doi.org/10.1016/j.addma.2019.100794
2. Akhoundi, B., Nabipour, M., Hajami, F., S. Band, S., Mosavi, A.: Calculating Filament Feed in the Fused Deposition Modeling Process to Correctly Print Continuous Fiber Composites in Curved Paths. Materials **13**, 4480 (10 2020). https://doi.org/10.3390/ma13204480
3. Anderegg, D.A., Bryant, H.A., Ruffin, D.C., Skrip, S.M., Fallon, J.J., Gilmer, E.L., Bortner, M.J.: In-situ monitoring of polymer flow temperature and pressure in extrusion based additive manufacturing. Additive Manufacturing **26**, 76–83 (2019). https://doi.org/10.1016/j.addma.2019.01.002
4. Babaei, V., Vidimce, K., Foshey, M., Kaspar, A., Didyk, P., Matusik, W.: Color contoning for 3D printing. ACM Transactions on Graphics **36**(4), 124:1–124:15 (2017). https://doi.org/10.1145/3072959.3073605
5. Bellini, A., Güçeri, S., Bertoldi, M.: Liquefier dynamics in fused deposition. Journal of Manufacturing Science and Engineering **126**(2), 237–246 (May 2004). https://doi.org/10.1115/1.1688377
6. Chermain, X., Zanni, C., Martínez, J., Hugron, P.A., Lefebvre, S.: Orientable dense cyclic infill for anisotropic appearance fabrication. ACM Transactions on Graphics **42**(4) (2023). https://doi.org/10.1145/3592412, to appear.
7. Comminal, R., Serdeczny, M.P., Pedersen, D.B., Spangenberg, J.: Numerical modeling of the strand deposition flow in extrusion-based additive manufacturing. Additive Manufacturing **20**, 68–76 (2018). https://doi.org/10.1016/j.addma.2017.12.013
8. Comminal, R., da Silva, W.R.L., Andersen, T.J., Stang, H., Spangenberg, J.: Influence of processing parameters on the layer geometry in 3D concrete printing: Experiments and modelling. Rilem State of the Art Reports pp. 852–862 (2020). https://doi.org/10.1007/978-3-030-49916-7_83

9. Comminal, R., Spangenberg, J., Hattel, J.H.: Cellwise conservative unsplit advection for the volume of fluid method. Journal of Computational Physics **283**, 582–608 (2015). https://doi.org/10.1016/j.jcp.2014.12.003
10. Flow Science, Inc: FLOW-3D® (2019), https://www.flow3d.com
11. Hergel, J., Lefebvre, S.: Clean color: Improving multi-filament 3D prints. Computer Graphics Forum **33**(2), 469–478 (2014). https://doi.org/10.1111/cgf.12318
12. Inc., X.: da Vinci Color 3D Printer. https://www.xyzprinting.com/en-US/product/da-vinci-color (2022)
13. Koirala, P., Hauta-Kasari, M., Martinkauppi, B., Hiltunen, J.: Color mixing and color separation of pigments with concentration prediction. Color Research & Application **33**(6), 461–469 (2008). https://doi.org/10.1002/col.20441
14. Kuipers, T., Elkhuizen, W., Verlinden, J., Doubrovski, E.: Hatching for 3D prints: Line-based halftoning for dual extrusion fused deposition modeling. Computers & Graphics **74**, 23–32 (2018). https://doi.org/10.1016/j.cag.2018.04.006
15. Littler, E., Zhu, B., Jarosz, W.: Automated filament inking for multi-color FFF 3D printing. In: ACM Symposium on User Interface Software and Technology (UIST). pp. 83:1–83:13 (2022). https://doi.org/10.1145/3526113.3545654
16. Mollah, M.T., Comminal, R., Serdeczny, M.P., Pedersen, D.B., Spangenberg, J.: Stability and deformations of deposited layers in material extrusion additive manufacturing. Additive Manufacturing **46**, 102193 (2021). https://doi.org/10.1016/j.addma.2021.102193
17. Mollah, M.T., Comminal, R., Serdeczny, M.P., Pedersen, D.B., Spangenberg, J.: Numerical predictions of bottom layer stability in material extrusion additive manufacturing. JOM **74**(3), 1096–1101 (2022). https://doi.org/10.1007/s11837-021-05035-9
18. Mollah, M.T., Moetazedian, A., Gleadall, A., Yan, J., Alphonso, W.E., Comminal, R.B., Seta, B., Lock, T., Spangenberg, J.: Investigation on corner precision at different corner angles in material extrusion additive manufacturing: An experimental and computational fluid dynamics analysis. International Solid Freeform Fabrication Symposium pp. 872–881 (2022). https://doi.org/10.26153/tsw/44202
19. Mueller, R.K.: Spiritdude's Public Notebook. https://spiritdude.wordpress.com/2019/04/11/ (2019)
20. Phan, D.D., Swain, Z.R., Mackay, M.E.: Rheological and heat transfer effects in fused filament fabrication. Journal of Rheology **62**, 1097–1107 (2018). https://doi.org/10.1122/1.5022982
21. Reiner, T., Carr, N., Měch, R., Šťava, O., Dachsbacher, C., Miller, G.: Dual-color mixing for fused deposition modeling printers. Computer Graphics Forum **33**(2), 479–486 (2014). https://doi.org/10.1111/cgf.12319
22. Serdeczny, M.P., Comminal, R., Mollah, M.T., Pedersen, D.B., Spangenberg, J.: Numerical modeling of the polymer flow through the hot-end in filament-based material extrusion additive manufacturing. Additive Manufacturing **36**, 101454 (2020). https://doi.org/10.1016/j.addma.2020.101454
23. Serdeczny, M.P., Comminal, R., Mollah, M.T., Pedersen, D.B., Spangenberg, J.: Viscoelastic simulation and optimisation of the polymer flow through the hot-end during filament-based material extrusion additive manufacturing. Virtual and Physical Prototyping **17**(2), 205–219 (2022). https://doi.org/10.1080/17452759.2022.2028522
24. Serdeczny, M.P., Comminal, R., Pedersen, D.B., Spangenberg, J.: Experimental and analytical study of the polymer melt flow through the hot-end in material extrusion additive manufacturing. Additive Manufacturing **32**, 100997 (2020). https://doi.org/10.1016/j.addma.2019.100997

25. Serdeczny, M.P., Comminal, R.B., Pedersen, D.B., Spangenberg, J.: Experimental validation of a numerical model for the strand shape in material extrusion additive manufacturing. Additive Manufacturing **24**, 145–153 (2018). https://doi.org/10.1016/j.addma.2018.09.022
26. Serdeczny, M.P., Comminal, R., Pedersen, D.B., Spangenberg, J.: Numerical prediction of the porosity of parts fabricated with fused deposition modeling. International Solid Freeform Fabrication Symposium pp. 1849–1854 (2018). https://doi.org/10.26153/tsw/17187
27. Song, H., Martínez, J., Bedell, P., Vennin, N., Lefebvre, S.: Colored fused filament fabrication. ACM Transactions on Graphics **38**(5), 141:1–141:11 (2019). https://doi.org/10.1145/3183793
28. Spangenberg, J., Leal da Silva, W.R., Mollah, M.T., Comminal, R., Juul Andersen, T., Stang, H.: Integrating reinforcement with 3D concrete printing: Experiments and numerical modelling. Rilem State of the Art Reports pp. 379–384 (2022). https://doi.org/10.1007/978-3-031-06116-5_56
29. Sukindar, N.A., Ariffin, M.K.A., Hang Tuah Baharudin, B.T., Jaafar, C.N.A., Ismail, M.I.S.: Analyzing the effect of nozzle diameter in fused deposition modeling for extruding polylactic acid using open source 3D printing. Jurnal Teknologi **78**(10), 7–15 (2016). https://doi.org/10.11113/jt.v78.6265
30. Takahashi, H., Punpongsanon, P., Kim, J.: Programmable filament: Printed filaments for multi-material 3D printing. In: ACM Symposium on User Interface Software and Technology (UIST). pp. 1209–1221 (10 2020). https://doi.org/10.1145/3379337.3415863
31. Tlegenov, Y., Hong, G.S., Lu, W.F.: Nozzle condition monitoring in 3D printing. Robotics and Computer-Integrated Manufacturing **54**, 45–55 (2018). https://doi.org/10.1016/j.rcim.2018.05.010
32. Tlegenov, Y., Lu, W.F., Hong, G.S.: A dynamic model for current-based nozzle condition monitoring in fused deposition modelling. Progress in Additive Manufacturing **4**, 211–223 (2019). https://doi.org/10.1007/s40964-019-00089-3
33. Valberg, A.: Light, Vision, Color. Wiley (2005)
34. W. Hirt, C., D. Nichols, B.: Volume of fluid (vof) method for the dynamics of free boundaries. Journal of Computational Physics **39**(1), 201–225 (1981). https://doi.org/10.1016/0021-9991(81)90145-5
35. Wang, Z., Shen, H., Wu, S., Fu, J.: Colourful fused filament fabrication method based on transitioning waste infilling technology with a colour surface model. Rapid Prototyping Journal **27**(1), 145–154 (2021). https://doi.org/10.1108/RPJ-04-2020-0072
36. Wu, L., Yang, T., Guan, Y., Shi, G., Xiang, Y., Gao, Y.: Semantic guided multi-directional mixed-color 3D printing. In: International Conference on Image and Graphics (ICIG), Lecture Notes in Computer Science, vol. 12890, pp. 106–117. Springer (2021). https://doi.org/10.1007/978-3-030-87361-5_9